Analysis of FO-CRS tomography Using Common-Shot Configuration: A Synthetic Data Study

Marcelo Jorge Luz Mesquita[1] and João Carlos Ribeiro Cruz[2]; [1]SEDUC/PA, [2]IG/UFPA

This paper was prepared for presentation during the 18th International Congress of the Brazilian Geophysical Society held in Rio de Janeiro, Brazil, 16-19 October 2023.

Abstract

The Finite-Offset Common-Reflection-Surface (FO-CRS) tomography is a fully automated methodology for inverting P-wave velocities using pre-stack seismic data. The inversion strategy is based on scanning semblance measurements in each common-midpoint gather, guided by the traveltime paraxial approximations of the FO-CRS method. By using the Very Fast Simulated Annealing (VFSA) optimization strategy, the proposed inversion algorithm aims to converge the objective function towards the global maximum, ensuring optimal estimation of the velocity model. In this study, we employ the seismic common-shot gather configuration, which utilizes a reduced number of FO-CRS parameters, to analyze the performance of the method.

Introduction

Accurate estimation of a velocity macro-model is crucial for reliable seismic interpretation of geological structures in oil and gas exploration. Various powerful methods, such as Tarantola (1984) and Virieux and Operto (2009), have gained popularity for velocity model estimation in complex geological environments. Nonetheless, seismic tomography continues to be an essential alternative for precise velocity inversion.

Coherency measurements have been utilized in efficient velocity inversion strategies employing global optimization techniques for several decades. These methods aim to find the velocity model that best predicts reflection events in beam-stacked data or through the use of stereotomography or Normal-Incidence-Point (NIP) tomography (Landa et al., 1988; 1989; Prieux et al., 2012; Köhn et al., 2016; Mesquita et al., 2019). These approaches offer distinct advantages, including their independence from pre-stack time picking and their ability to avoid time data fitting.

In the FO-CRS tomography strategy (Mesquita et al., 2019), the inversion process initiates with the interpretation of seismic reflections on the time-migrated seismic section. Each interpreted horizon is converted to depth using an initial velocity model and image rays. A set of finite-offset central rays is then constructed through selected layers for a group of Common Midpoint (CMP) gathers along the model. Using the FO-CRS traveltime approximation (Jäger, 1999; Zhang et al, 2001; Garabito et al, 2011) and guided by the CMP gathers, coherency measurements are calculated using semblance as the objective function. Layer by layer, the interval velocities are optimized using the VFSA algorithm (Ingber, 1989) to maximize the semblance objective function. The VFSA algorithm ensures velocity updates even when semblance values are relatively low, based on a probability criterion.

In this study, we analyze the performance of FO-CRS tomography by applying it to a synthetic dataset using the seismic common-shot gather configuration. This configuration offers the advantage of using a reduced number of FO-CRS parameters. Additionally, we examine the convergence of the method by analyzing semblances with different configurations.

Method

FO-CRS traveltime

The travel time of the finite-offset paraxial ray, known as the finite-offset CRS stacking operator, can be expressed as follows for a central ray that starts at *S* with an initial velocity v_S and a starting angle β_S, reflects at *R* in the subsurface, and emerges at the surface in *G* with a final velocity v_G and an emergence angle β_G. This expression assumes $v_S = v_G = v_0$ and is based on the work of Zhang et al. (2001):

$$T_{CRS}^2 = \left[t_0 + \left(\frac{1}{v_0}\right)(a_1\Delta x_m + a_2\Delta h)\right]^2 + \left(\frac{t_0}{v_0}\right)[a_3 - a_4]\Delta x_m^2 - \left(\frac{t_0}{v_0}\right)[a_4 - a_5]\Delta h^2 + 2\left(\frac{t_0}{v_0}\right)[a_4 + a_5]\Delta x_m \Delta h. \quad (1)$$

The parameters in the expression are related as follows: $a_1 = \sin\beta_G + \sin\beta_S$, $a_2 = \sin\beta_G - \sin\beta_S$, $K = 4K_1 - 3K_3$, $a_3 = K\cos^2\beta_G$, $a_4 = K_2\cos^2\beta_S$, and $a_5 = K_3\cos^2\beta_G$. Here, t_0 represents the travel time along the central ray, while β_S and β_G correspond to the start and emergence angles of the central ray at the positions of the source *S* and the receiver *G*, respectively. $\Delta x_m = x_m - x_0$ and $\Delta h = h - h_0$ represent the midpoint and half-offset displacements, where $x_0 = (x_G + x_S)/2$ is the midpoint and $h_0 = (x_G - x_S)/2$ is the half-offset of the central ray with finite-offset. The quantities x_m and h represent the

coordinates of an arbitrary paraxial ray with finite-offset. The wave velocities at the source *S* and receiver *G* are given by v_S and v_G, respectively. K_1, K_2 and K_3 are the wavefront curvatures associated with the central ray, which are calculated at the respective emergence points (Garabito et al., 2011).

For the common-shot (CS) condition, where the sources of the paraxial and central rays always coincide, the $\Delta x_m = \Delta h$ condition holds true. In this case, the FO-CRS traveltime approximation can be expressed as follows:

$$t^2(\Delta h) = \left[t_0 + 2\frac{\sin\beta_G}{v_G}\Delta h\right]^2 + 4t_0\left[k_1\frac{\cos^2\beta_G}{v_G}\right]\Delta h^2\,, \quad (2)$$

where it depends on the two attributes k_1 and β_G (Garabito et al., 2011).

FO-CRS tomography (CS gather case)

Starting with an initial depth-velocity model and a well-interpreted migrated seismic section, we identify the desired reflection time horizons. Utilizing an image ray time-to-depth converter, we obtain a set of model parameters represented by the vector $\mathbf{m} = \{\mathbf{Z}, \mathbf{V}\}$, which encompasses the velocity values and layer interfaces in the depth model. The interface node vector $\mathbf{Z} = \mathbf{Z}(\mathbf{V})$ is a function of the velocity vector in each layer. To determine the optimal $\mathbf{m} = \{\mathbf{Z}, \mathbf{V}\}$, we maximize the coherency calculated for all pre-stack trace gathers within a time window along traveltime trajectories, layer by layer (Mesquita et al., 2019). Figure 1 shows the flowchart of the step-by-step of the FO-CRS tomography method by considering the CS gather as the pre-stack input.

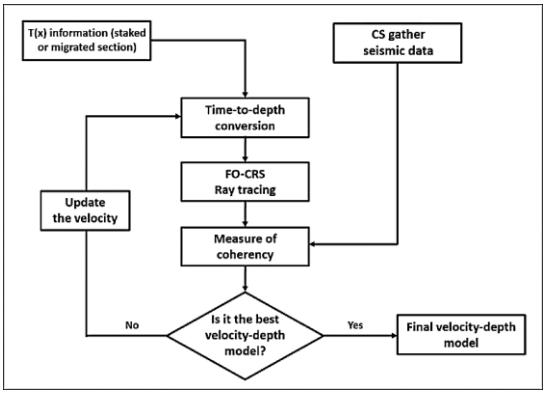

Figure 1. Flowchart showing the step-by-step of the FO-CRS tomography method using the CS gather configuration.

Coherence measurement: Semblance

Semblance (Neidell and Taner, 1971) is a commonly employed coherence measurement in the seismic stack process. It assesses the presence or absence of signals that exhibit correlation along the traveltime curves, which are calculated using the FO-CRS approximation. In the context of FO CRS tomography applications, the semblance function can be expressed as follows:

$$S_2(\mathbf{m}) = \frac{\sum_{k=-w}^{w}\left[\sum_{i=1}^{N} a_i(t_k)\right]^2}{N\sum_{k=-w}^{w}\left[\sum_{i=1}^{N} a_i(t_k)^2\right]}\,. \quad (3)$$

In this case, the vector of parameters m is represented as $\mathbf{m} = \{\mathbf{V}, \mathbf{Z}(\mathbf{V}), \mathbf{W}(\mathbf{V}, \mathbf{Z})\}$, where $\mathbf{V}$ is the velocity vector, $\mathbf{Z}$ is the depth vector, and $\mathbf{W} = (t_o, K_2, K_3, \beta_s, \beta_g)$. The seismic signal amplitude $a_i(t_k)$ is indexed by the trace order number i and the time t. The time index k falls within a specified time window of width $2w + 1$. The semblance function yields a value between 0 and 1, with values closer to 1 indicating a better obtained model.

In the FO CRS tomography strategy, the objective function $E(\mathbf{m})$ is defined as the arithmetic mean of all semblance values calculated within a layer (Mesquita et al., 2019). It can be expressed as:

$$E(\mathbf{m}) = \frac{1}{L}\sum_{j=1}^{L}[S(\mathbf{m})]_j\,. \quad (4)$$

Here, L represents the number of CMP gathers analyzed per layer.

In this study, for the purpose of comparing the convergence of the method, we will use a modified version of the semblance function (Mesquita et al., 2021), given by:

$$\hat{S}_m(\mathbf{m}) = 1 - \frac{\sum_{k=-w}^{w}\left[\sum_{i=1}^{N}(a_{ik} - \mathrm{M})^m\right]}{\sum_{k=-w}^{w}\left[\sum_{i=1}^{N} a_{ik}^m\right]}. \quad (5)$$

where $a_{ik} = a_i(t_k)$, m is the order of the equation, and M is the median of a set of amplitudes along the FO CRS traveltime curve.

Application

We implemented our proposed approach to a synthetic geological model consisting of three homogeneous layers with velocities $v_1 = 1500$ m/s, $v_2 = 1800$ m/s, and $v_3 = 2100$ m/s, as illustrated in Figure 2. The yellow dashed line indicates the location of the analyzed CS gathers. In our simulation, the minimum and maximum offsets were 25 m and 1475 m, respectively, with 30 geophones spaced at 50 m intervals. We utilized the FO-CRS central ray with half offset for the analysis.

For this example, we analyzed six common-shots per layer, both with and without the inclusion of noise, with a signal-to-noise ratio (SNR) of 3 dB. Figure 3 illustrates two examples of the first ten traces from the second shot, one without (a) and another with noise (b). In our convergence analysis, we considered both the conventional semblance and the modified semblance with median. Finally, we estimated the velocity model using FO-CRS tomography with the CS configuration in three cases: employing the second order semblance (conventional), the second order with median, and the fourth-order with median. In the inversion examples using VFSA, the search range for the

first layer was set between 1300 m/s to 1700 m/s, while for the second layer, it was between 1600 m/s and 2000 m/s.

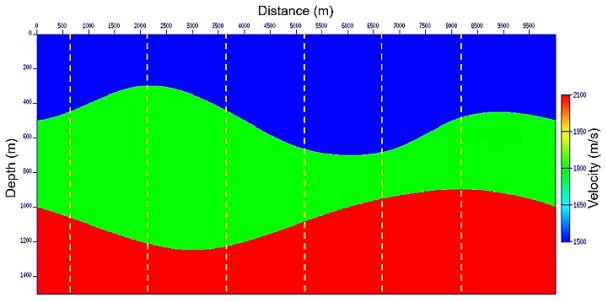

Figure 2: The synthetic velocity model comprises three layers with the following velocities: v_1 = 1500 m/s, v_2 = 1800 m/s, and v_3 = 2100 m/s. The dashed lines indicate the shot positions. The minimum and maximum offsets are 25 m and 1475 m, respectively, with 30 geophones spaced at intervals of 50 m.

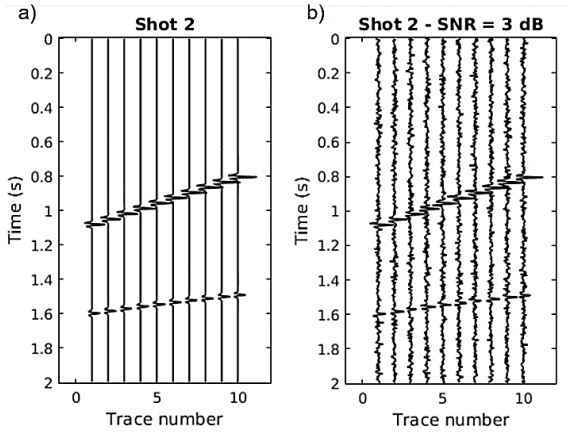

Figure 3: Examples of the first ten traces from the second shot, illustrating the cases without (a) and with (b) the addition of noise.

Results

In the first part of the analysis, we examined the maximum semblance-velocity pairs for each shot throughout the model by scanning velocities with 2 m/s increments within the range of 1200 m/s to 1800 m/s for the first layer, and 5 m/s increments within the range of 1600 m/s to 2000 m/s for the second layer. Table 1 presents the results of the analysis using the second-order conventional semblance serving as the objective function, with a noise-free dataset. Similarly, Table 2 presents the same experiment with the inclusion of noise in the dataset. This comparison revealed minimal variation in the results with and without noise for some shots. However, for others, this variation reached around 45 m/s. This also indicate that the curvature of the interfaces and the structural complexity of the medium can affect the obtained values in each region of the model.

The convergence test was performed using the noisy dataset, with a focus on the first layer. Two different semblance functions were considered: the conventional second-order semblance and the second-order semblance with median. Figures 4 and 5 illustrate the results for 10 analyses for each semblance. The standard deviations acquired for the estimated velocities in each case were 5.5821 m/s and 3.4423 m/s, respectively. In other words, the semblance with median provided greater uniformity in the results.

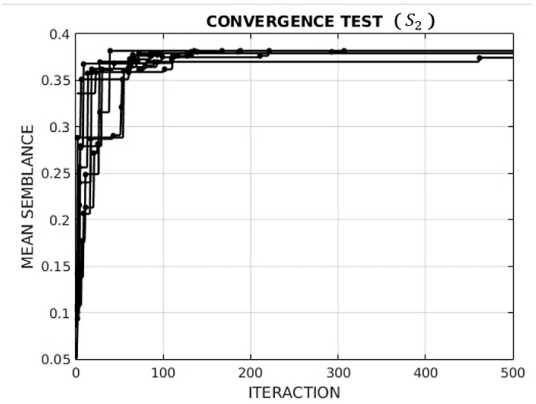

Figure 4: Convergence analysis for 10 tests and 500 iterations in the first layer using the second-order conventional semblance as the objective function. In this case, the standard deviation of the estimated velocities was 5.5821 m/s, with a search range between 1300 m/s and 1700 m/s.

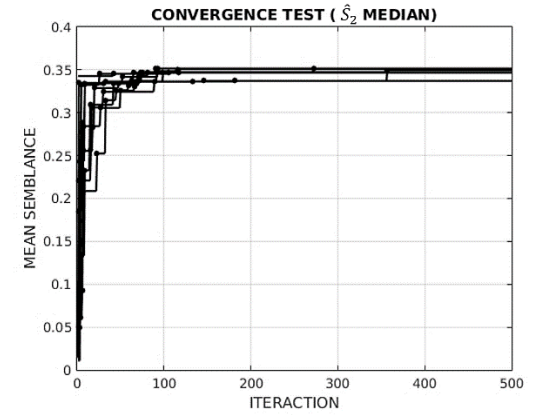

Figure 5: Convergence analysis for 10 tests and 500 iterations in the first layer using the second-order semblance with median as the objective function. In this case, the standard deviation of the estimated velocities was 3.4423 m/s, with a search range between 1300 m/s and 1700 m/s.

The results of the final test, using FO-CRS tomography with the CS configuration, and adding noise to the dataset, are presented in Figures 6 and 7. Figure 6 illustrates the model with the initial velocities of layers 1 and 2, v_1 = 1300 m/s and v_2 = 1600 m/s, respectively. Figure 7 shows the estimated final model after 100 iterations, with velocities v_1 = 1477 m/s and v_2 = 1777 m/s. Tests were also conducted with second- and fourth-order semblance with median. For these two cases, the obtained velocities were $v_1 = 1483$ m/s and $v_2 = 1808$ m/s; and $v_1 = 1483$ m/s and $v_2 = 1778$ m/s, respectively, indicating velocities slightly closer to the exact values.

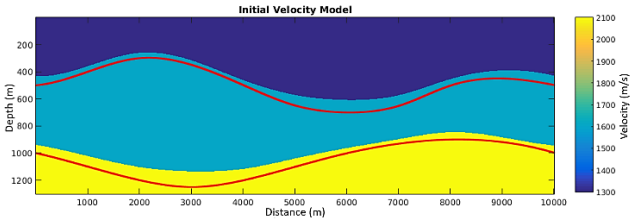

Figure 6: Initial velocity model, with the red curves representing the exact interface positions. v_1 = 1300 m/s and v_2 = 1600 m/s.

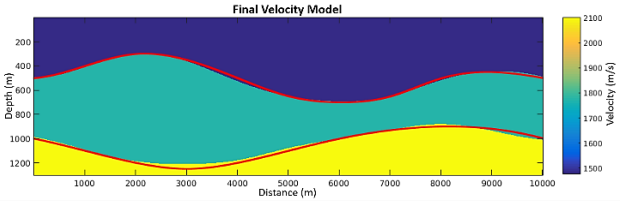

Figure 7: Estimated velocity model after 100 iterations, with the red curves representing the exact interface positions. v_1 = 1477 m/s and v_2 = 1777 m/s.

Table 1. Results of the shot-by-shot analysis using the second-order conventional semblance as the objective function for the noise-free dataset.

	Shot 1	Shot 2	Shot 3	Shot 4	Shot 5	Shot 6
Layer 1	$v_1 = 1478$ m/s $S_2 = 0.8990$	$v_1 = 1516$ m/s $S_2 = 0.3816$	$v_1 = 1474$ m/s $S_2 = 0.6656$	$v_1 = 1484$ m/s $S_2 = 0.4894$	$v_1 = 1506$ m/s $S_2 = 0.6050$	$v_1 = 1456$ m/s $S_2 = 0.7551$
Layer 2	$v_2 = 1760$ m/s $S_2 = 0.8216$	$v_2 = 1785$ m/s $S_2 = 0.7272$	$v_2 = 1800$ m/s $S_2 = 0.8953$	$v_2 = 1790$ m/s $S_2 = 0.9064$	$v_2 = 1795$ m/s $S_2 = 0.9040$	$v_2 = 1840$ m/s $S_2 = 0.8694$

Table 2. Results of the shot-by-shot analysis using the second-order conventional semblance as the objective function for the noisy dataset.

	Shot 1	Shot 2	Shot 3	Shot 4	Shot 5	Shot 6
Layer 1	$v_1 = 1478$ m/s $S_2 = 0.8812$	$v_1 = 1516$ m/s $S_2 = 0.3877$	$v_1 = 1504$ m/s $S_2 = 0.2397$	$v_1 = 1484$ m/s $S_2 = 0.4886$	$v_1 = 1506$ m/s $S_2 = 0.5641$	$v_1 = 1456$ m/s $S_2 = 0.7346$
Layer 2	$v_2 = 1765$ m/s $S_2 = 0.7731$	$v_2 = 1740$ m/s $S_2 = 0.5860$	$v_2 = 1800$ m/s $S_2 = 0.7916$	$v_2 = 1800$ m/s $S_2 = 0.8359$	$v_2 = 1770$ m/s $S_2 = 0.8002$	$v_2 = 1795$ m/s $S_2 = 0.8066$

Conclusions

This study presented a brief investigation of FO-CRS tomography using the common-shot configuration, including an analysis of different semblance functions, convergence, and the inversion of a synthetic velocity model. The results indicate that the method performs effectively with the proposed configuration, providing the advantage of employing only two FO-CRS parameters compared to other source-receiver configurations. Different objective functions were also evaluated, highlighting a slightly advantage of second-order semblance with median. Additionally, the addition of noise did not significantly affect the results, as evidenced by the examples.

Acknowledgments

The authors would like to thank the Geophysical Graduate Course of the Federal University of Pará for supporting this research.

References

Garabito, G., Oliva, P. C., Cruz, J. C. R., 2011, Numerical analysis of the finite-offset common-reflection-surface traveltime approximation. Journal of Applied Geophysics, 74, p. 89-99.

Ingber, L., 1989, Very fast simulated reannealing. Mathl. Comput. Modeling 12(8), 967-993.

Jäger, R., 1999, The common-reflection-surface stack-theory and application. Master's thesis. Universität Karlsruhe (Germany).

Köhn, D.; Nil, D.; Rabbel, W. Estimation of long-wavelength initial models for seismic full waveform inversion – Part 2 CRS-Stack and NIP-wave tomography. 76th annual meeting of the German Geophysical Society (DGG), 2016.

Landa, E.; Kosloff, D.; Keydar, S.; Koren, Z.; Reshef, M., 1988, A method for determination of velocity and depth from

seismic reflection data. Geophysical Prospecting, 36, p. 223-243.

Landa, E.; Beydoun, W.; Tarantola, A., 1989, Reference velocity model estimation from prestack waveforms: Coherency optimization by simulated annealing. Geophysics, v.54, n. 8, p. 984-990.

Mesquita, M. J. L., Cruz, J. C. R., Callapino, G. G., 2019, Velocity inversion by global optimization using finite-offset common-reflection-surface stacking applied to synthetic and Tacutu Basin seismic data. Geophysics, v. 84(2), p. R165-R174.

Mesquita, M, J. L., Cruz, J. C. R., 2021, Analysis of an alternative semblance function applied to Finite-Offset Common-Reflection-Surface tomography. 17th International Congress of the Brazilian Geophysical Society.

Neidell, N. S.; Taner, M. T., 1971, Semblance and other coherency measures for multichannel data. Geophysics, v. 36, p. 482-497.

Prieux, V.; Lambarè, G.; Operto, S.; Virieux, J. Building starting models for full waveform inversion from wide-aperture data by stereotomography. Geophysical Prospecting, p. 1-29, 2012.

Tarantola, A., 1984, Inversion of seismic reflection data in the acoustic approximation. Geophysics, v. 49, p. 1259-1266.

Virieux, J., and Operto, S., 2009, An overview of full-waveform inversion in exploration geophysics. Geophysics, v. 74, n. 6, p. WCC1-WCC26.

Zhang, Y.; Bergler, S.; Tygel, M.; Hubral, P., 2001, Common-Reflection-Surface (CRS) stack for common-offset. Geophy. Prospect. 49, 709-718.